

# My, how you've grown: a practical guide to modeling size transitions for Integral Projection Model (IPM) applications

Tom E.X. Miller<sup>\*a</sup> and Stephen P. Ellner<sup>b</sup>

<sup>a</sup>Department of BioSciences, Rice University, Houston, TX

<sup>b</sup>Department of Ecology and Evolutionary Biology, Cornell University,  
Ithaca, New York

**Running header:** Better growth modeling for IPMs

---

\*Corresponding author. Department of BioSciences, Rice University, Houston, TX 77005-1827. Email:  
tom.miller@rice.edu Phone: 713-348-4218

<sup>1</sup> **Abstract**

<sup>2</sup>    1.

<sup>3</sup>    2.

<sup>4</sup>    3.

<sup>5</sup>    4.

<sup>6</sup> **Keywords**

## 7 Introduction

8 Structured demographic models – matrix and integral projection models (MPMs and  
9 IPMs) – are powerful tools for data-driven modeling of population dynamics and viabil-  
10 ity that are widely used in basic and applied settings. In contrast to MPMs for popula-  
11 tions with discrete structure (life stage, age class, etc.), IPMs (Easterling et al., 2000) read-  
12 ily accommodate populations structured by continuous state variables, most commonly  
13 size. A related innovation of the IPM framework is its emphasis on regression-based  
14 modeling for parameter estimation, which carries important advantages for making the  
15 most of hard-won data (Ellner et al., 2022).

16 A standard workflow allows ecologists to assemble an IPM from data using famili-  
17 iar statistical tools to describe growth, survival, reproduction, and other demographic  
18 transitions as functions of size (Coulson, 2012; Ellner et al., 2016). The relative ease of  
19 the regression-based approach, accommodating multiple covariates (e.g., environmental  
20 factors, experimental treatments) and complex variance structures (e.g., random effects,  
21 correlated errors), has facilitated a growing body of IPM literature that examines how  
22 biotic or abiotic factors affect population dynamics (e.g., Louthan et al., 2022; Ozgul  
23 et al., 2010; Schultz et al., 2017) and explores the consequences of demographic hetero-  
24 geneity associated with spatial, temporal, and individual variation (e.g., Compagnoni  
25 et al., 2016; Crone, 2016; Plard et al., 2018). The vital rate regressions (or “sub-models”)  
26 are the bridge between the individual-level data and the population-level model and its  
27 predictions; it is important to get them right.

28 Compared to other vital rates, growth is special. The regression sub-models for  
29 survival and reproduction provide the expected values of those rates as functions of  
30 size (we use “size” as the name for whatever continuous variable defines the population  
31 structure, which could instead be immune competence, mother’s weight, etc.). However,  
32 for modeling growth, the full probability distribution of subsequent size, conditioned on  
33 initial size, must be defined. This distribution defines the growth ‘kernel’  $G(z', z)$  that  
34 gives the probability density of any future size  $z'$  at time  $t + 1$  conditional on current size  
35  $z$  at time  $t$ . Whenever survival and reproduction are size-dependent, the entire distribu-  
36 tion of size transitions can strongly influence IPM predictions because this distribution  
37 governs how frequently size changes are much greater or much lower than average.

38 The original template for modeling size transitions in IPMs was provided by East-  
39 erling et al. 2000. They first tried simple linear regression, assuming normally dis-  
40 tributed size changes with constant variance. Because the residuals from this regression  
41 exhibited non-constant variance, they used a two-step approach that estimated the size-

42 dependence in the growth variance (better options soon became available, such as the  
43 `lme` function in R). However, even after accounting for non-constant variance, growth  
44 data may still deviate from the assumption that size transitions are normally distributed.  
45 Size transitions are often skewed such that large decreases are more common than large  
46 increases (Peterson et al., 2019; Salguero-Gómez and Casper, 2010), or vice versa (Stub-  
47 berud et al., 2019). Size transitions may also exhibit excess kurtosis ('fat tails'), where  
48 extreme growth or shrinkage is more common than predicted by the tails of the normal  
49 distribution (Hérault et al., 2011).

50 The observation that the normal distribution may poorly describe size transitions  
51 in real organisms has been made before, and several studies have emphasized that al-  
52 ternative distributions should be explored (Easterling et al., 2000; Peterson et al., 2019;  
53 Rees et al., 2014; Williams et al., 2012). Yet, default use of Gaussian growth distribu-  
54 tions (often with non-constant variance) remains the standard practice. An ISI Web of  
55 Knowledge search on the terms 'integral projection model ecology' (DATE) returned #  
56 IPM studies published in the past decade (2010–2020), # of which assumed a Gaussian  
57 growth kernel.<sup>1</sup> The general state-of-the-art in the literature appears to remain where it  
58 was 20 or so years ago, using the default model without pausing to examine critically  
59 whether or not it actually provides a good description of the data. We are guilty of this,  
60 ourselves.

61 The persistence of Gaussian growth modeling is understandable. There is a long  
62 tradition of statistical modeling built on the assumption of normally distributed residu-  
63 als with constant variance. Popular software packages such as `lme4` (Bates et al., 2007)  
64 and `MCMCglmm` (Hadfield et al., 2010) make it easy to fit growth models with po-  
65 tentially complex fixed- and random-effect structures, but the possible distributions of  
66 continuous responses are limited, and default to Gaussian. Abandoning these conve-  
67 nient tools for the sake of more flexible growth modeling means, it may seem, sacrificing  
68 the flexibility to rigorously model diverse and potentially complex sources of variation  
69 in growth, some of which may be the motivation driving the study in the first place.

70 The question we address here is: how can ecologists escape the apparent trade-off  
71 between realistically capturing the variance, skew, and kurtosis of size transition data  
72 on the one hand, and flexibly including the multiple covariates and random effects that  
73 often have substantial impacts on demographic rates. In this article, we offer an answer.

74 Our goal here is to present and illustrate a general 'recipe' that moves growth mod-  
75 eling past the standards set over 20 years ago. Like any recipe, users may need to  
76 make substitutions or add ingredients to suit their situation. Our approach emphasizes

---

<sup>1</sup>I still intend to do this! But it's a rabbit hole I have not gone down yet.

77 graphical diagnostics for developing and evaluating growth models, rather than a pro-  
78 cess centered on statistical model selection. Through a set of empirical case studies we  
79 demonstrate how a simple workflow, using tools that were nonexistent or not readily  
80 available when IPMs first came into use, makes it straightforward and relatively easy to  
81 identify when the default model is a poor fit to the data, and to then choose and fit a  
82 substantially better growth model that is no harder to use in practice. We illustrate our  
83 approach by revisiting four of our own, mostly published IPM analyses that assumed  
84 Gaussian growth.<sup>2</sup> In each case, the Gaussian assumption does not stand up to close  
85 scrutiny. We illustrate how we could have done better, and the consequences of “doing  
86 better” for our ecological inferences. All of our analyses may be reproduced from code  
87 and data that are publicly available (see Data accessibility statement).

## 88 A general workflow for better growth modeling

89 The modeling workflow that we suggest runs as follows (Fig. 1):

- 90 1. *Fit a “pilot” model or models assuming a Gaussian distribution but allowing for non-*  
91 *constant variance.*

92 This step is familiar to most IPM users, as it is the start and end of the traditional  
93 workflow. A well-fitted Gaussian model accurately describes the mean and variance  
94 of future size conditional on current size and possibly on other measured covariates  
95 or random effects. This step may include model selection to identify which treat-  
96 ment effects or environmental drivers affect the mean and/or variance of future size.  
97 Non-constant variance is often fitted in a two-stage process, first fitting mean growth  
98 assuming constant variance, then doing a regression relating the squared residuals  
99 from the initial fit to the fitted mean. It is sometimes better to fit size-dependence  
100 in the mean and variance simultaneously, as can be done with the R packages **mgcv**  
101 and **nmle**, because incorrectly assuming constant variance can affect the outcome of  
102 model selection for the mean. One-step fitting is straightforward for simple models  
103 in which initial size is the only factor that can influence growth variance. However,  
104 the two-step process fitting residuals to the fitted value (expected future size) may  
105 be convenient when there are multiple fixed and random effects, all of which may  
106 contribute to non-constant variance, since the expected value implicitly accounts for  
107 all of them. We illustrate both one-step and two-step approaches in the examples  
108 below.

---

<sup>2</sup>Need to commit to case study choices - Steve wanted to include corals for contrast with Peterson et al.

109 Allowing non-constant variance means that it is not necessary to transform the  
110 data in a way that stabilizes the growth variance. Transformation remains an option  
111 when it does not create new problems (see Discussion), and it may have advantages  
112 besides variance stabilization. In particular log-transformation is often appropriate  
113 for size data (Ellner et al., 2016), and it helps avoid eviction at small sizes.

- 114 2. *Use statistical and graphical diagnostics to identify if and how the standardized residuals*  
115 *deviate from Gaussian, and to identify a more appropriate distribution.*

116 If the Gaussian pilot model is valid, the set of standardized residuals (standardized  
117 by the standard deviation) should be Gaussian with mean zero and unit variance,  
118 with no skew or excess kurtosis. This criterion provides a straightforward test for  
119 whether to accept a Gaussian growth model or explore alternatives. If the standard-  
120 ized residuals are satisfactorily Gaussian, skip to the final step of the workflow.

121 There are many ways that growth data may deviate from Gaussian, and the nature  
122 of those deviations can guide the search for a better distribution. Frequentist  
123 tests such as the D'Agostino test of skewness (D'Agostino, 1970) and the Anscombe-  
124 Glynn test of kurtosis (Anscombe and Glynn, 1983) could be used to diagnose  
125 whether the aggregate distribution of standardized residuals deviates from normal-  
126 ity (R package **moments** (Komsta and Novomestky, 2015)). However, the aggregate  
127 distribution of standardized residuals may be misleading if properties such as skew  
128 and kurtosis vary with size. For example, a change in the direction of skewness from  
129 small to large sizes would require a distribution flexible enough to accommodate  
130 both positive and negative skew, such as the skewed normal or Johnson  $S_U$  distri-  
131 butions. Alternatively, growth data may lack skew but may exhibit leptokurtosis (in  
132 which case the  $t$  distribution may be a good choice) or may shift from platykurtosis  
133 to leptokurtosis depending on initial size (in which case the power exponential  
134 distribution may be a good choice). It is therefore essential to visualize trends in dis-  
135 tribution properties with respect to size, either initial size (for simple models with  
136 only size-dependence) or expected future size (for models with multiple fixed ef-  
137 fects). In the case studies below, we rely on quantile regression of the standardized  
138 residuals to visualize skew and kurtosis as continuous functions of size or expected  
139 value. Fig. 1 includes guidance on how the skew and kurtosis properties of the stan-  
140 dardized residuals suggest options for an appropriate growth distribution. In our  
141 case studies we take advantage of the many distributions provided in the **gamlss** R  
142 package (Stasinopoulos et al., 2007), but any other distributions with the necessary  
143 properties can be used.

144 3. *Refit the growth model using the chosen distribution.*

145 In models with multiple covariates and/or random effects, each potentially affecting  
146 several distribution parameters (location, scale, skew, kurtosis) in different ways,  
147 “refit the model” could entail a massive model selection process to identify the  
148 “right” or “best” non-Gaussian model. And with so many options, model uncer-  
149 tainty may be overwhelming and over-fitting becomes a significant risk even if pre-  
150 cautions against it are taken. We therefore argue for adopting the more modest  
151 goal of remedying the apparent defects in the Gaussian model. Conveniently, as  
152 we demonstrate below, the functional forms for the mean and standard deviation  
153 (or location and scale parameters) could be carried over from the pilot Gaussian  
154 model into a non-Gaussian distribution, leaving skew and kurtosis as the targets for  
155 improvement. This step exploits the fact that parameter estimation from a Gaus-  
156 sian model is generally robust to deviations from normality (Schielzeth et al., 2020),  
157 meaning that the mean of the Gaussian model is probably a good proxy for the mean  
158 of the non-Gaussian model (and in case it is not, the next step in the workflow would  
159 catch that). The functional forms for skew and kurtosis of the non-Gaussian model  
160 can be guided by the qualitative features of the graphical diagnostics (e.g., skewness  
161 switches from positive to negative with size).

162 4. *Test the final model through graphical diagnostics comparing simulated and real growth data.*

163 A good model will generate simulated data that look like the real data. Again, it is  
164 important to inspect the properties of simulated data conditional on present size or  
165 expected future size, rather than examining the entire distribution. We provide ex-  
166 amples below of informative comparisons between simulated and real data, based  
167 mainly on quantiles. If the simulated data do not correspond well with real data,  
168 alternative (possibly more flexible) growth distributions should be explored, or more  
169 complex functions relating distribution parameters to current size and other covari-  
170 ates. However, we again caution against launching a full-blown model selection  
171 exercise. Instead, possible alternative models could be chosen primarily to remedy  
172 observable discrepancies between the real and simulated size transition data, and at  
173 most slightly modified based on final diagnostic and statistical tests.

## 174 How should skewness and kurtosis be measured?

175 “Improvement” of a Gaussian model will always involve scrutiny of skewness and kur-  
176 tosis, so measurement of these properties warrants some attention. The standard mea-

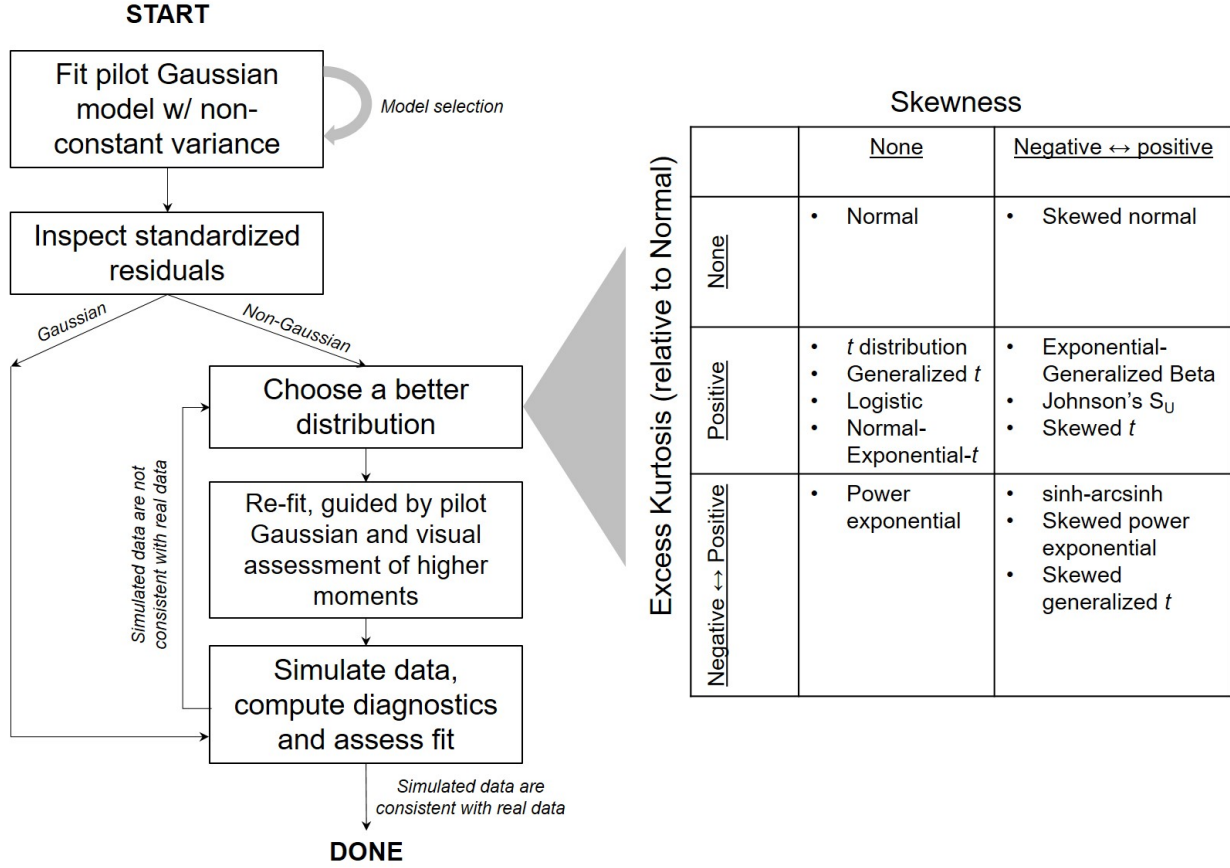


Figure 1: General workflow of recommendations for IPM growth modeling (left) and guide to common non-Gaussian distributions of size  $x$  for  $x \in \mathbb{R}$  that can accommodate different combinations of skewness and kurtosis (right). All of these distributions (often including multiple versions or parameterizations of each) are available in the package **gamlss.dist**, except for the skewed generalized *t*, which is available in the package **sgt** (Davis, 2015).

<sup>177</sup> sures of skewness and kurtosis (tail thickness) are based on the third and fourth central  
<sup>178</sup> moments, respectively, of the distribution:

$$\text{Skewness} = \frac{m_3}{\sigma^3}, \quad \text{Excess kurtosis} = \frac{m_4}{\sigma^4} - 3 \quad (1)$$

<sup>180</sup> where  $m_k = \mathbb{E}(X - \bar{X})^k$  is the  $k^{th}$  central moment of a random quantity  $X$  and  $\sigma^2$  is the  
<sup>181</sup> variance (second central moment). A Gaussian distribution has zero skewness and zero  
<sup>182</sup> excess kurtosis.

<sup>183</sup> The standard measures are easy to calculate but their use for choosing and eval-  
<sup>184</sup> uating growth models is hindered by their poor sampling properties. Because empirical  
<sup>185</sup> estimates involve high powers of data values, it only takes a few outliers to produce



Figure 2: Histograms of skewness and kurtosis estimates using moment-based definitions, compared with the nonparametric measures. Histograms are based on 5000 replicate draws of a sample of 200 independent values from a  $t$  distribution with 8 degrees of freedom. Dotted red vertical lines mark the minimum and maximum of sample estimates, and dashed blue lines show the 5th and 95th percentiles. The true value is indicated by a black dot on the  $x$ -axis. Figure drawn by script `NPmoments.R`

186 a very inaccurate estimate. Figure 2 shows a simulated example, where the underlying  
 187 “data” are a sample of size 200 from a  $t$  distribution with 8 degrees of freedom; the true  
 188 skew is 0, and the true excess kurtosis is 1.5. The distance between the largest and small-  
 189 est estimates (indicated by the dotted red vertical lines), relative to the distance between  
 190 the 5th and 95th percentiles, shows the broad extent of extreme values that can occur  
 191 even with a good size sample, especially for kurtosis.

192 We therefore use “nonparametric” (NP) measures of skew and kurtosis that are  
 193 based on quantiles and thus less sensitive to a few extreme data values. Let  $q_\alpha$  denote  
 194 the  $\alpha$  quantile of a distribution or sample (e.g.,  $q_{0.05}$  is the 5th percentile). For any  
 195  $0 < \alpha < 0.5$ , a quantile-based measure of skewness is given by (McGillivray, 1986)

$$196 \text{NP Skewness} = \frac{q_\alpha + q_{1-\alpha} - 2q_{0.5}}{q_{1-\alpha} - q_\alpha}. \quad (2)$$

197 NP Skewness is a measure of asymmetry between the tails of the distribution above and  
 198 below the median. The size of the upper tail can be measured (for any  $0 < \alpha < 0.5$ ) by  
 199  $\tau_U = q_{1-\alpha} - q_{0.5}$ ; for  $\alpha = 0.05$  this is the difference between the 95th percentile and the  
 200 median. The lower tail size is  $\tau_L = q_{0.5} - q_\alpha$ . The definition above is equivalent to

$$201 \quad \text{NP Skewness} = \frac{\tau_U - \tau_L}{(\tau_U + \tau_L)}. \quad (3)$$

202 So an NP Skewness of  $\pm 0.2$  says that the difference in tail sizes is 20% of their total. The  
 203 range of possible values is -1 to 1. Both  $\alpha = 0.25$  (sometimes called “Kelly’s skewness”)  
 204 and  $\alpha = 0.1$  (“Bowley’s skewness”) are common choices. We used  $\alpha = 0.1$ , unless  
 205 otherwise stated.

206 An analogous quantile-based measure of kurtosis (Jones et al., 2011) is

$$207 \quad \text{NP Kurtosis} = \frac{q_{1-\alpha} - q_\alpha}{q_{0.75} - q_{0.25}}. \quad (4)$$

208 For  $\alpha = 0.05$ , NP Kurtosis is the difference between the 95th and 5th percentiles, relative  
 209 to the interquartile range. To facilitate interpretation, we scale NP Kurtosis relative to  
 210 its value for Gaussian distribution, and subtract 1. We call this “NP Excess Kurtosis”.  
 211 The value for a Gaussian distribution is zero. A value of 0.2 means that the tails are (on  
 212 average) 20% heavier than those of a Gaussian with the same interquartile range, and  
 213 a value of -0.2 means that the tails are (on average) 20% lighter than a Gaussian with  
 214 the same interquartile range. We calculate NP Kurtosis using  $\alpha = 0.05$  unless otherwise  
 215 stated, to focus on the tail edges, but again this is somewhat arbitrary.

216 Figure 2C,D illustrate how, applied to exactly the same simulated samples, the non-  
 217 parametric measures of skewness and kurtosis produce a smaller fraction of highly in-  
 218 accurate estimates caused by a few extreme values in the sample. But also note that, in  
 219 contrast to the moment-based measures, numerically small values of the NP measures  
 220 (e.g., 0.1 or 0.2) should not be disregarded, because they are both scaled so that a value  
 221 of 1 indicates extremely large departures from a Gaussian distribution.

222 Quantile-based estimation of skewness and kurtosis carries the added value that  
 223 quantile regression methods may be used to derive these properties of size transitions  
 224 as continuous functions of initial size or expected future size. In the examples below,  
 225 we use the **qgam** package to fit smooth additive quantile regression models, which have  
 226 the flexibility to accommodate non-linear size-dependence in skewness and kurtosis.  
 227 One risk of a gam-based approach is that fitted quantiles may be too “wiggly” without  
 228 constraints on their complexity (in the examples below, we specify  $k = 4$  to constrain the

dimension of the basis function). For the gam-averse, other quantile regression models may be equally suitable. For consistency with non-parametric skewness and kurtosis, we similarly use quantile-based measures of mean and variance and quantile regression to visualize these as functions of size. Specifically, following Wan et al. (2014),

$$\text{NP Mean} = \frac{q_{0.25} + q_{0.5} + q_{0.75}}{3} \quad (5)$$

and

$$\text{NP SD} = \frac{q_{0.75} - q_{0.25}}{1.35}. \quad (6)$$

## 1 Case study: Sea fan corals, *Gorgonia ventalina*

We begin with a simple example where current size is the only predictor of future size. Bruno et al. (2011) developed an IPM to understand the rise and fall of a fungal pathogen *Aspergillus sydowii* in Caribbean sea fan corals *G. ventalina*. The model was based on repeated observations of marked corals in permanent transects at several sites near Akumal, Mexico, recording disease status (infected/uninfected) and the area of uninfected tissue. The epidemic peak had passed and disease incidence was already low, so infected fans were relatively infrequent. We therefore limit the analysis here to uninfected individuals. Bruno et al. (2011) found statistically significant year and site effects, but as those explained a very small fraction of the variation in growth increments, they fitted a single growth model to data pooled across years and sites. We do the same here. The pooled data set consists of 358 observed size transitions. The data exhibited size-dependent variance in growth (change in area,  $cm^2$ ), which Bruno et al. (2011) chose to stabilize by transforming size, using the cube-root of total fan area as the size measure (fig. ??B), and then fitting the standard model with Gaussian growth increments. Here we take a different approach, modeling size-dependent variance explicitly rather than trying to transform it away.

We develop a model using natural log transformation of area. With initial size as the only predictor, a simple way to fit a Gaussian model with nonconstant variance is the `gam` function in `mgcv` library (Wood, 2017) using the `gaulss` family. The mean and standard deviation are both fitted as smoothing spline functions of initial size, and the `predict` function returns the fitted mean and also the inverse of the fitted standard deviations with which we can compute the scaled residuals:

```
# XH is a data frame holding the data
# logarea.t0, .t1 denote initial and final values of log-transformed area
```

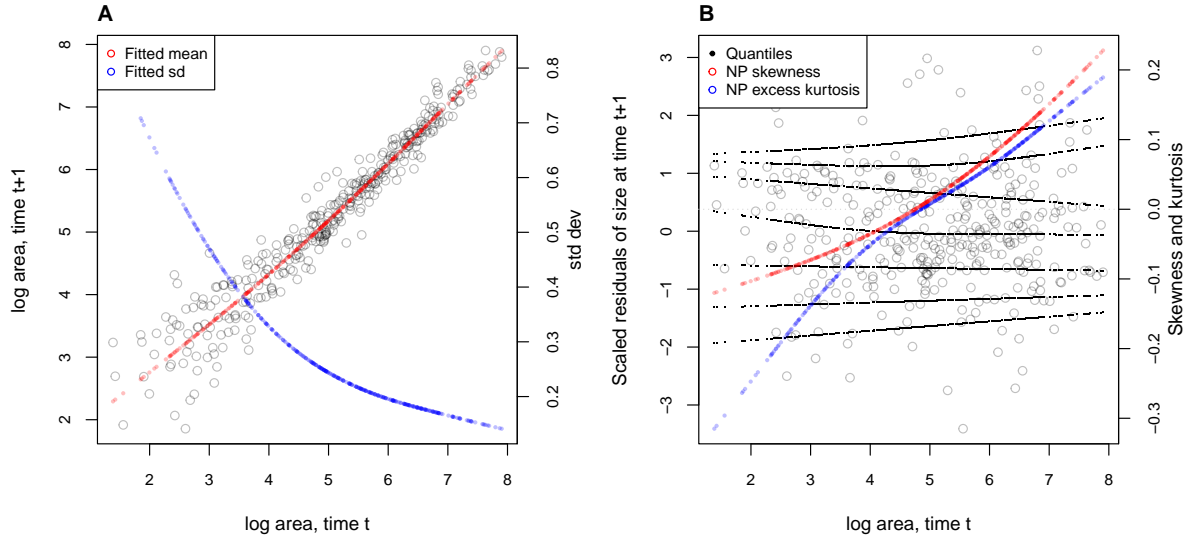


Figure 3: **A**, Size transition data for sea fan corals, *Gorgonia ventalina*, and fitted gam with mean (red) and standard deviation (blue) of future size conditional on current size. **B**, Quantile regressions of scaled residuals on size and nonparametric estimates of skewness (red) and excess kurtosis (blue) derived from them. Black lines in **B** show the 5th, 10th, 25th, 50th, 75th, 90th, and 95th quantiles. Figure made by script AkumalCorals\_qgam.R.

```

261 fitGAU <- gam(list(logarea.t1~ s(logarea.t0), ~ s(logarea.t0)),
262   data=XH, gamma=1.4, family=gaulss())
263 fitted_all = predict(fitGAU,type="response");
264 fitted_sd = 1/fitted_all[,2];
265 scaledResids = residuals(fitGAU,type='response')/fitted_sd;

```

Fig. 3A shows the log-transformed data and Gaussian model. The mean function (solid blue curve) is visually nearly linear, but the fitted nonlinear spline is strongly favored over a linear model for the mean ( $\Delta AIC \approx 9$ ). The spline for standard deviation  $\sigma$  versus initial size shows that smaller individuals exhibit greater variability in future size.

There are no blatant signs of trouble in the pilot Gaussian model, but quantile regressions on the scaled residuals, and the NP Skewness and Kurtosis metrics derived from them (Eq. 3 and 4), suggest deviations from normality (Fig. 3B). Specifically, skewness switches from negative to positive across the size distribution, with smaller corals more likely to shrink than grow and larger corals more likely to grow than shrink. Kurtosis also changes direction over the size distribution, with smaller initial sizes having thinner tails and larger initial sizes having fatter tails than Gaussian. The fitted nonparametric moments suggest that the upper and lower tails of size transition proba-

278 bilities may differ by up to 20%, and the weight of the tails may be 20% greater or less  
279 than Gaussian, depending on initial size – not overwhelming deficiencies, but not trivial  
280 either. Are these deviations from normality severe enough to warrant a second, non-  
281 Gaussian iteration of growth modeling? This question may be answered by simulating  
282 data from the Gaussian model and examining whether key properties of the simulated  
283 data are consistent with those of the real data – this is the ultimate litmus test for a  
284 growth model’s adequacy and should be a standard element of IPM construction, in our  
285 opinion. If the simulated data are not consistent with the real data, it is time to choose  
286 a better distribution (Fig. 1). In this case, the negative skew at small sizes and excess  
287 kurtosis observed at large sizes are more extreme than what occurs across 100 random  
288 iterations of data simulation (Fig. 4), suggesting that, for at least some parts of the size  
289 distribution, a non-Gaussian model would better capture size transitions.

290 We sought a distribution that could accommodate the properties of the scaled resid-  
291 uals, specifically changes in the sign of skewness and excess kurtosis across initial sizes.  
292 We chose the sinh-arcsinh (SHASH) distribution, a four-parameter distribution that, con-  
293 veniently, is included in **mcmc**’s **gam()** function:

```
294 fitSHASH <- gam(list(logarea.t1 ~ s(logarea.t0,k=4), # <- location  
295 ~ s(logarea.t0,k=4), # <- log-scale  
296 ~ s(logarea.t0,k=4), # <- skewness  
297 ~ s(logarea.t0,k=4)), # <- log-kurtosis  
298 data = XH, family = shash, optimizer = "efs")
```

299 Data simulated from this model are more consistent with the real data than the Gaussian  
300 model: many of the 100 simulated SHASH data sets exhibited negative skew at small  
301 sizes and positive excess kurtosis at large sizes that were as strong or stronger than  
302 observed in the real data (Fig. 4). If one cared to quantify the difference between models,  
303 the SHASH is clearly favored by AIC despite having twice as many parameters as the  
304 Gaussian ( $\Delta AIC = 7.04$ ).

305 What, then, have we gained by fitting a better growth model? Fig. 5A compares  
306 the predicted distributions of subsequent size in the fitted model and Gaussian pilot  
307 models, for the median size of a new recruit (leftmost pair of curves), the median initial  
308 size (central curves), and the 95th percentile of initial size in the data (rightmost curves).  
309 The differences are small, and most pronounced for the smallest size, where recruits  
310 are predicted to grow slightly larger under the SHASH model than the Gaussian model.  
311 The direction of this difference was surprising, since the SHASH accommodates negative  
312 skew at small sizes in the data. However, in modeling skew appropriately, the SHASH

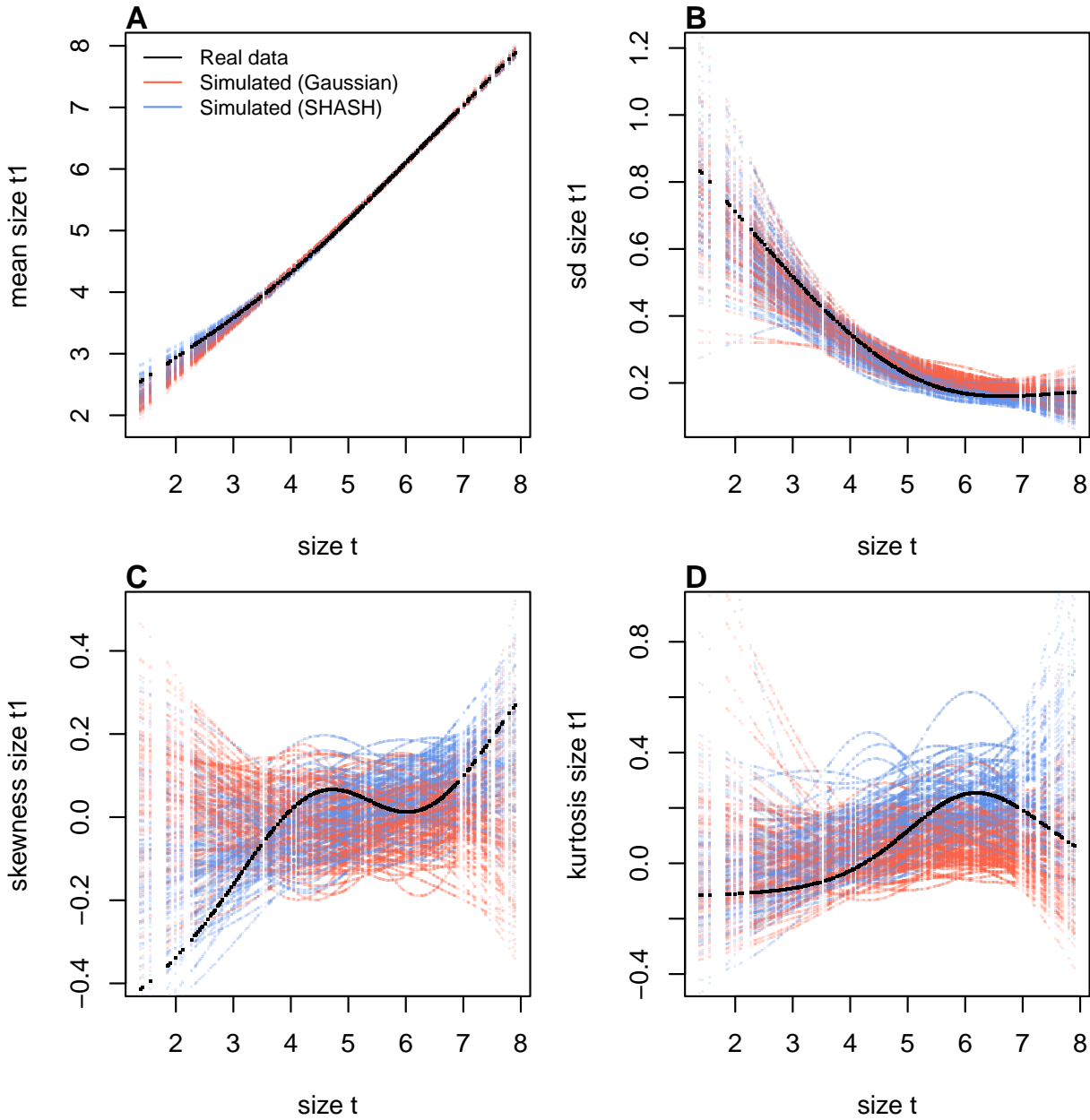


Figure 4: Comparisons among real coral data and data simulated from Gaussian and SHASH growth models for mean, standard deviation, NP skewness, and NP kurtosis of future size conditional on current size. Figure made by script `AkumalCorals_qgam.R`.

model also gives a better prediction for mean growth at small sizes than the Gaussian model, whose mean is biased downward by negative skew (Fig. 4A)<sup>3</sup>. Something similar happens in the standard deviation at large sizes (log size 5–7), where excess kurtosis in the data biased the SD upward (Fig. 4B). Fig. 5B shows the predicted steady-state size

<sup>3</sup>...Contradicting the earlier assertion that parameter estimates from Gaussian models are robust to deviations from normality!

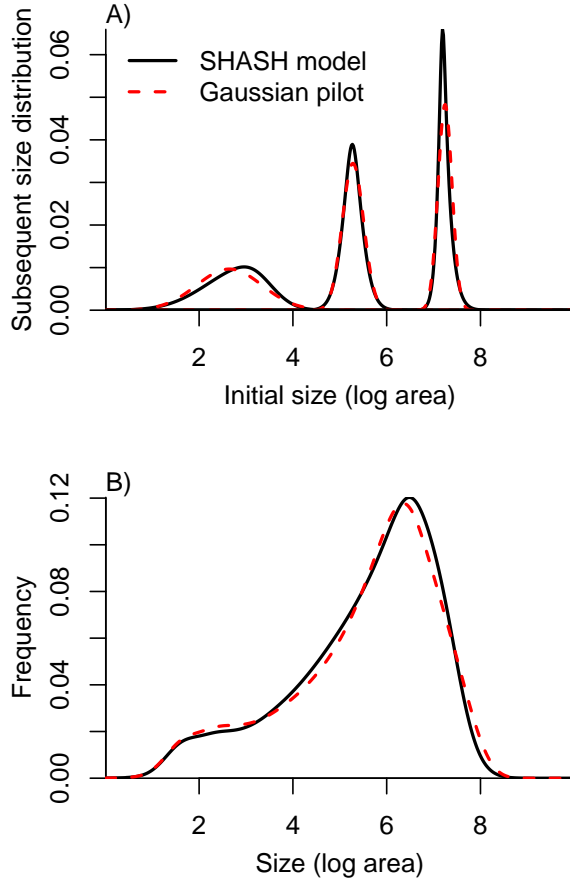


Figure 5: Comparisons between the fitted SEP1 growth model (solid black curves) and the Gaussian pilot model (dashed red curves) for sea fans *G. ventalina*. A) Predicted frequency distributions of size in year  $t + 1$  for three different values of size in year  $t$ . The leftmost pair of curves are for initial size equal to the median size of a new recruit (data from (Bruno et al., 2011)); central pair is for the median initial size of uninfected individuals; rightmost pair are for the 95th percentile initial size for uninfected individuals. B) Steady-state size distributions resulting from a constant unit input of new recruits. As in Bruno et al. (2011) we assume that larvae are very widely dispersed, so that the number of recruits arriving at any one location is independent of the local population abundance or structure. Size distribution of recruits was described by a kernel density estimate based on the (sadly, only  $n = 9$ ) measured sizes of known new recruits. Figure made by script AkumalCoralsIPMs.R.

317 distributions resulting from a constant unit input of recruits. Again, the differences are  
 318 very subtle. Finally, the Gaussian and SHASH growth models predict very similar mean  
 319 life span (17.7 and 17.9 years, respectively). From these outputs, there is little evidence  
 320 that improved modeling of coral growth meaningfully improved biological inferences  
 321 from the IPM; one could argue that it was not worth the trouble.

322 In this case study we used `gam` to fit both the Gaussian and SHASH models because  
323 that obviated model selection on functions for mean, variance, and higher moments.  
324 However, `gam` should be used with caution. Nonparametric regression models notori-  
325 ously “wag their tails” because the ends of the fitted curve can be pulled close to the  
326 outermost data points. This is especially problematic for growth modeling, because data  
327 are typically sparse near the bounds of the size distribution. To minimize the risk of  
328 overfitting we specified the number of “knots” (`k=4`) and used `gamma=1.4` to overweight  
329 model degrees of freedom, as suggested by Gu (2013, sec. 3.2). But it is always impor-  
330 tant to plot the fitted splines and make sure they do not wag unrealistically. If they do,  
331 parametric regression may be a better choice.

## 332 2 Case study: tree cholla cactus, *Cylindriopuntia imbricata*

333 The next case study, focusing on the tree cholla cactus *Cylindriopuntia imbricata* at the  
334 Sevilleta Long-Term Ecological Research site in central New Mexico, adds a new feature  
335 on top of the simple size-dependent regressions in the previous study: random effects  
336 associated with temporal (year) and spatial (plot) environmental heterogeneity. This  
337 long-term study of cactus demography was initiated in 2004 and different subsets of  
338 the data have been analyzed in various IPM studies, all using Gaussian growth kernels  
339 (Compagnoni et al., 2016; Czachura and Miller, 2020; Elderd and Miller, 2016; Miller  
340 et al., 2009; Ohm and Miller, 2014). In fact, (Elderd and Miller, 2016) presented a Gaus-  
341 sian growth model fit to the cactus data as an example of a well fit growth function,  
342 based on a marginal distribution of residuals that appeared approximately Gaussian  
343 and posterior predictive checks (PPCs) of a Bayesian model that suggested consistency  
344 between the real data and data simulated from the fitted model (Fig. 4 in (Elderd and  
345 Miller, 2016)). While PPCs and the associated “Bayesian P-value” are popular diagnostic  
346 tools, they are often considered to be too conservative (Conn et al., 2018; Zhang, 2014),  
347 failing to reject marginally bad models even though they are very effective in rejecting  
348 models that are terrible. The choice of discrepancy function (the statistic used to com-  
349 pare real and simulated data) can also be limiting: in our previous work, we used a  
350 discrepancy function focused on variance (the sum of the squared residuals), so we had  
351 a built-in blind-spot for mismatches in higher moments. In the clarity of hindsight, the  
352 PPC gave a false sense of security; the Gaussian was a poor choice all along.

353 The data for this new analysis include 4844 size transition observations from 929 in-  
354 dividuals spanning 13 transition years (2004–2018) and 11 spatial replicates (three spatial  
355 blocks in years 2004–2008 and eight 30m-by-30m plots in years 2009–2018). The data are  
356 provided in Miller (2020). Following previous studies, we quantified size as the natural  
357 logarithm of plant volume ( $cm^3$ ), derived from height and width measurements.

358 We begin the growth modeling workflow, as above, with a generalized additive  
359 model with the mean and standard deviation of size in year  $t + 1$  modeled as function  
360 of size in year  $t$ , with random intercepts for year and plot and assuming normally dis-  
361 tributed residuals (`family=gaulss()`). The standardized residuals, accounting for size-  
362 dependent residual variance (Fig. 6A), show clear signals of negative skew and positive  
363 excess kurtosis across most of the size distribution but strongest in the middle of the size  
364 distribution (Fig. 6B).

365 To better capture size transitions, we need a distribution with negative skew and  
366 positive excess kurtosis, but both of which may be negligible at some sizes. We first tried

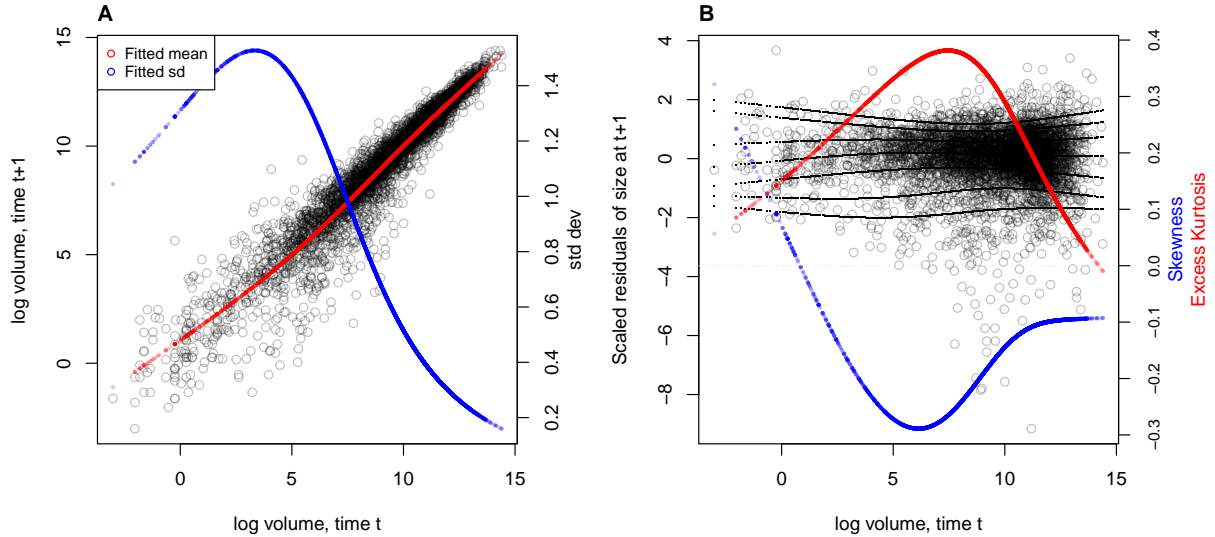


Figure 6: **A**, Size transition data for tree cholla cacti, *Cylindropuntia imbricata*, and fitted gam with mean (red) and standard deviation (blue) of future size conditional on current size. **B**, Quantile regressions of scaled residuals on size and nonparametric estimates of skewness (red) and excess kurtosis (blue) derived from them. Black lines in **B** show the 5th, 10th, 25th, 50th, 75th, 90th, and 95th quantiles. Figure made by script `cactus_growth_modeling_qgam.R`.

367 Johnson's  $S_U$  and then the skewed  $t$  distributions, both of which are limited to positive  
 368 excess kurtosis. Both distributions provided some improvement over the Gaussian, but  
 369 were not happy with the fit of either. Iterating through the workflow (Fig. 1), we ar-  
 370 rived, again, at the SHASH distribution, which is more flexible than either the JSU or  
 371 skewed  $t$ , capable of capturing a greater range of kurtosis for a given amount of skew,  
 372 and vice versa (Steve's NPSkewKurtosisRanges.pdf). Furthermore, fitting the SHASH  
 373 as a generalized additive model with `mgcv` allowed for flexible, non-monotonic size-  
 374 dependence in skewness and kurtosis without the need for model selection on specific  
 375 size-dependent functions; through iterations of trial and error, we found this flexibility  
 376 was necessary to generate simulated data that compared favorably to the real data. The  
 377 other distributions that we tried are not available as `mgcv` families, so we fit these with  
 378 custom maximum likelihood functions, an approach we illustrate in the next case study.  
 379 The final growth model was similar to the SHASH gam in the coral case study, but  
 380 with random intercepts for the location parameter, representing spatial and temporal  
 381 heterogeneity:

```
382 fit_shash <- gam(list(logvol_t1 ~ s(logvol_t,k=4) +  

  383 s(plot,bs="re") + s(year_t,bs="re")), # <- model for locat
```

```

384 ~ s(logvol_t,k=4), # <- model for log-scale
385 ~ s(logvol_t,k=4), # <- model for skewness
386 ~ s(logvol_t,k=4)), # <- model for log-kurtosis
387 data = CYIM_grow,
388 family = shash,
389 optimizer = "efs")

```

390 The final SHASH model provided good correspondence between simulated and  
391 real data, and provided more compelling improvement over the Gaussian model than  
392 we saw in the coral case study (Fig. 7). The SHASH model over-estimated negative  
393 skew at some sizes relative to the signal of skewness in the data (Fig. 7C), but the nature  
394 of size-dependent skew in the data is not very biologically plausible and may instead  
395 be driven by the tail-wagging tendency of gams. As in the coral case study, we see  
396 that correctly modeling skewness and kurtosis improved estimation of the mean and  
397 standard deviation (Fig. 7A,B), yielding a growth model that is clearly truer to the data  
398 than the pilot Gaussian fit.

399 We explored how improved growth modeling influenced IPM results, leveraging  
400 the plot and year structure of the study design to quantify spatial and temporal vari-  
401 ance in fitness. The structure and parameterization of the full IPM are described in  
402 Appendix XX. We used the fitted random effects from the vital rate models to estimate  
403 the asymptotic growth rate for each year ( $\lambda_t$ ), centered on the average plot, and for  
404 each plot ( $\lambda_p$ ), centered on the average year. This allowed us to quantify demographic  
405 variance associated with temporal and spatial heterogeneity. We found that the Gaus-  
406 sian growth model tended to over-estimate  $\lambda_t$ , particularly in the harshest years (Fig.  
407 8A), and thus under-estimated temporal variance in fitness ( $Var(\lambda_{t(Gaussian)}) = 0.0018$ ,  
408  $Var(\lambda_{t(SHASH)}) = 0.0023$ ). The opposite was true for plot-to-plot variation (Fig. 8B),  
409 where the Gaussian model under-estimated  $\lambda_p$  and over-estimated spatial variance in  
410 fitness ( $Var(\lambda_{p(Gaussian)}) = 0.00015$ ,  $Var(\lambda_{p(SHASH)}) = 0.000088$ ). Across both growth  
411 models, fluctuations in fitness were stronger through time than across space. The  
412 difference in temporal variance would suggest that Gaussian growth modeling would  
413 lead to over-estimation of the stochastic growth rate  $\lambda_S$ , since temporal variance has  
414 a negative influence on  $\lambda_S$ . However, this was not the case: stochastic IPMs based  
415 on Gaussian and SHASH growth models had nearly identical stochastic growth rates  
416 ( $\lambda_S(Gaussian) = 0.9906$ ,  $\lambda_S(SHASH) = 0.9909$ ). This is likely because temporal fluctu-  
417 ations in vital rates, which is where the SHASH growth model would make a difference,  
418 have a weaker influence on  $\lambda_S$  than the temporal fluctuations in size structure that they

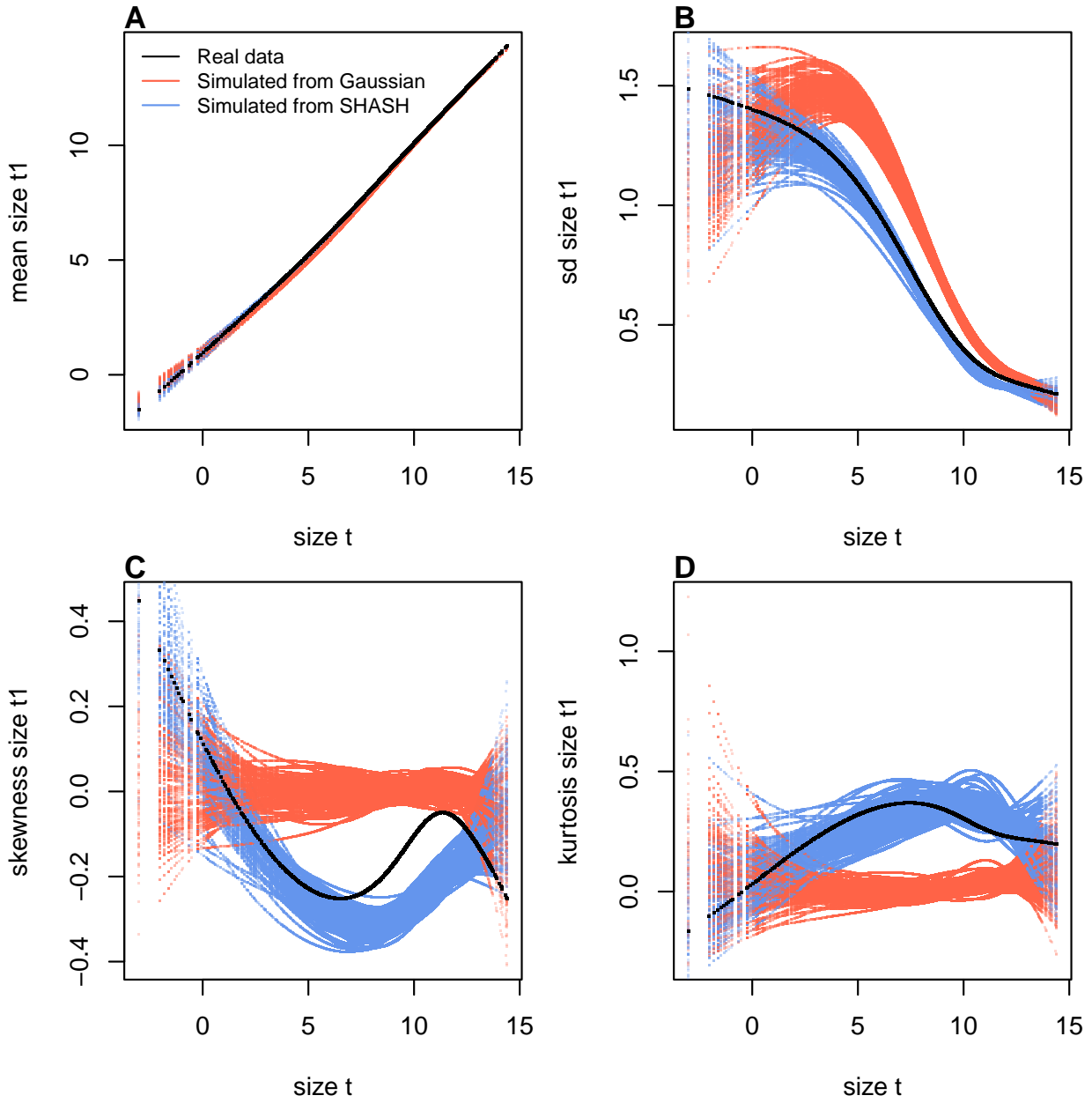


Figure 7: Comparisons among real cactus data and data simulated from Gaussian and SHASH growth models for mean, standard deviation, NP skewness, and NP kurtosis of future size conditional on current size. Figure made by script `cactus_growth_modeling_qgam.R`.

<sup>419</sup> generate (Compagnoni et al., 2016; Ellis and Crone, 2013). Thus, depending on the target  
<sup>420</sup> of one's analysis, modeling non-Gaussian size transitions with a Gaussian growth model  
<sup>421</sup> could bias results in either direction, or make no difference at all.

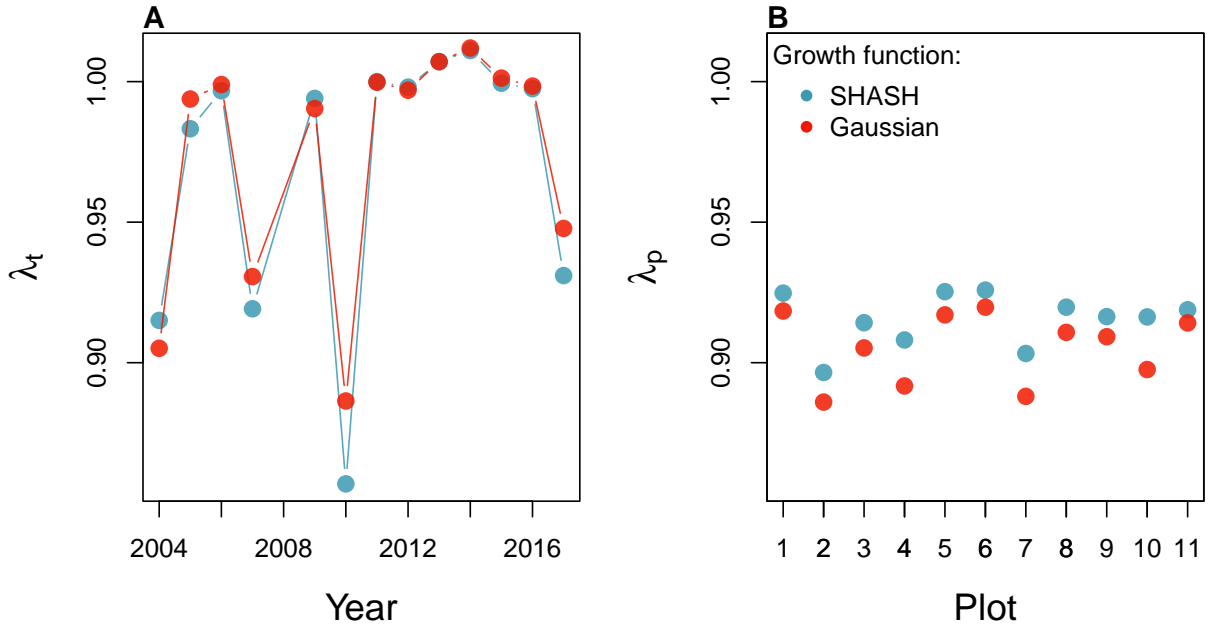


Figure 8: .

### 422 3 Case study: creosotebush, *Larrea tridentata*

423 Our next case study comes from our studies of the woody shrub creosotebush (*Larrea tri-*  
 424 *dentata*) at the Sevilleta Long-Term Ecological Research (LTER) site in central New Mex-  
 425 ico, US. At this site as elsewhere in the Southwest US, creosotebush is encroaching into  
 426 desert grassland habitats. The data described here were collected along transects span-  
 427 ning grass-shrub ecotones to understand patterns of density dependence in creosotebush  
 428 demography. Specifically, we asked whether fitness is maximized approaching zero den-  
 429 sity at the leading edge of the expansion front (consistent with ‘pulled’ expansion), or  
 430 whether there is a demographic advantage for shrubs at higher density due to positive  
 431 feedbacks expected for ecosystem engineers (leading to ‘pushed’ expansion). Our pub-  
 432 lished study (Drees et al., 2023) used a spatial integral projection model (SIPM) to predict  
 433 the speed of shrub encroachment, assuming normally-distributed size transitions. Here  
 434 we step through our suggested workflow to ask whether a non-Gaussian model would  
 435 have been more faithful to the data, and how such an improvement would influence  
 436 predictions for the speed of encroachment. We use this case study to illustrate several  
 437 new elements and challenges, including modeling skewness and kurtosis as functions  
 438 of expected future size (instead of initial size) and using distributions that are not cur-  
 439 rently available as **mgcv** families. In fact, to diversify our use of software and illustrate  
 440 alternatives, we do not use gam’s for any element of this case study.

441 Growth data come from 522 shrubs censused longitudinally over four years (2013-  
442 2017). Census individuals occurred along 12 replicate transects (200 to 600 m in length)  
443 that spanned gradients of shrub density along shrub-grass ecotones. Size was measured  
444 as volume of an elliptical cone based on height and width measurements; the size vari-  
445 able of the IPM was the natural logarithm of volume ( $cm^3$ ). For each census individual,  
446 we recorded the size and density of all conspecifics within the five-meter transect “win-  
447 dow” in which it occurred, and took the sum of all sizes within the window as a measure  
448 of local density. The data are available in Ochocki et al. (2023).

449 As an initial Gaussian approach, we first fit a set of candidate generalized linear  
450 mixed models, including transect as a random effect, that represented competing hy-  
451 potheses for how size, density, and their interaction influence growth. Specifically, we fit  
452 five candidate Gaussian models that included fixed effects of initial size only (model 1),  
453 size and density (model 2), and size, density, and their interaction (model 3), allowing  
454 for shrubs of different sizes to have different growth responses to local density. Models  
455 4 and 5 mirrored models 2 and 3 but included second-order terms for density, allowing  
456 for the possibility of non-monotonic density dependence. As in (Drees et al., 2023) we  
457 pooled data across three transition years. Initial AIC rankings of these pilot models fa-  
458 vor model 4 slightly over model 5 ( $\Delta AIC = 0.8$ ) and significantly over all other models  
459 ( $\Delta AIC > 2$ ). However, these models were fit assuming constant variance, and inspection  
460 of the residuals of the best model indicate this is not a safe assumption.

461 Unlike our previous case studies, here we have multiple fixed effects that may influ-  
462 ence the variance of future size. In cases such as this, we recommend modeling variance  
463 as a function of expected future size rather than initial size, as we did with the corals  
464 and cacti. The expected (or “fitted”) values reflect the combined influence of all fixed  
465 and random effects, and therefore implicitly account for multiple sources of variation in  
466 the variance. While there are several convenient software packages for simultaneously  
467 modeling Gaussian mean and variance as functions of independent variables (**mgcv** for  
468 additive models as we saw above, **nmle** for linear models), modeling variance as a func-  
469 tion of the mean is trickier because they cannot easily be fit simultaneously. Here we  
470 us an iterative re-weighting approach – which is not elegant, but it works. For Gaus-  
471 sian models, weights  $w_i$  can be used to indicate that the observations  $y_i$  vary in their  
472 dispersion around the mean. In general, the iterative steps are:

1. Fit the expected value and normally-distributed residuals with constant variance:

$$y_i = \mu_i + \epsilon_i$$

$$\epsilon_i \sim N(0, \sigma)$$

2. Fit the standard deviation of the residuals as a function of the expected value.  
Weights are derived as the inverse of the fitted variance:

$$\epsilon_i \sim N(0, f(\mu_i))$$

$$w_i = 1/f(\mu_i)^2$$

3. Re-fit the observation model, weighting the residual variance according to step 2:

$$y_i = \mu_i + \epsilon_i$$

$$\epsilon_i \sim N(0, \sigma \times \sqrt{w_i})$$

473 We iterated steps 2 and 3 until the weights did not change. In step 2, we modeled  
474 the standard deviation as a simple linear function of the expected value ( $\log(f(\mu_i)) =$   
475  $\beta_0 + \beta_1 * \mu_i$ ) but other functions are possible, as is model selection among them. We  
476 did this for all candidate models and, for fair AIC comparison, we re-fit all candidate  
477 models with the same weights, estimated from the top model. The updated model  
478 selection continued to favor model 4, but now with a stronger improvement over the  
479 next-best model ( $\Delta AIC = 3.0$ ). The code that executes our iterative re-weighting can be  
480 found in SCRIPT.

481 The resulting Gaussian growth model accounts for non-constant variance through  
482 the fitted weights, which indicate greater dispersion for smaller values of expected size  
483 ( $\beta_1 = -0.21$ ). Quantiles of the standardized residuals of this model indicate weak neg-  
484 ative skew (difference in tail size is 1–2% of their total) and positive excess kurtosis,  
485 especially at smaller expected sizes (tails are 6–10% fatter than Gaussian) (Fig. 9). <sup>4</sup>  
486 As a candidate for improvement, we turned to the Johnson's  $S_U$  (JSU) distribution, a  
487 four-parameter, leptokurtic distribution capable of skew in either direction. We used  
488 a parameterization of the JSU for which location parameter  $\mu$  is the mean and scale  
489 parameter  $\sigma$  is the standard deviation (Rigby et al., 2019).

490 Like many of the non-Gaussian candidates that we suggest (Fig. 1), the JSU dis-  
491 tribution is not presently available as a family option for linear mixed models in any  
492 software package, to our knowledge. However, this need not be a barrier to using it for

---

4 Note that there is still a variance trend in the standardized residuals—rather unsatisfying! I have been through this backwards and forwards and my take is that this is a product of the sample size imbalance between small and large plants. The quantile regression is doing its best.

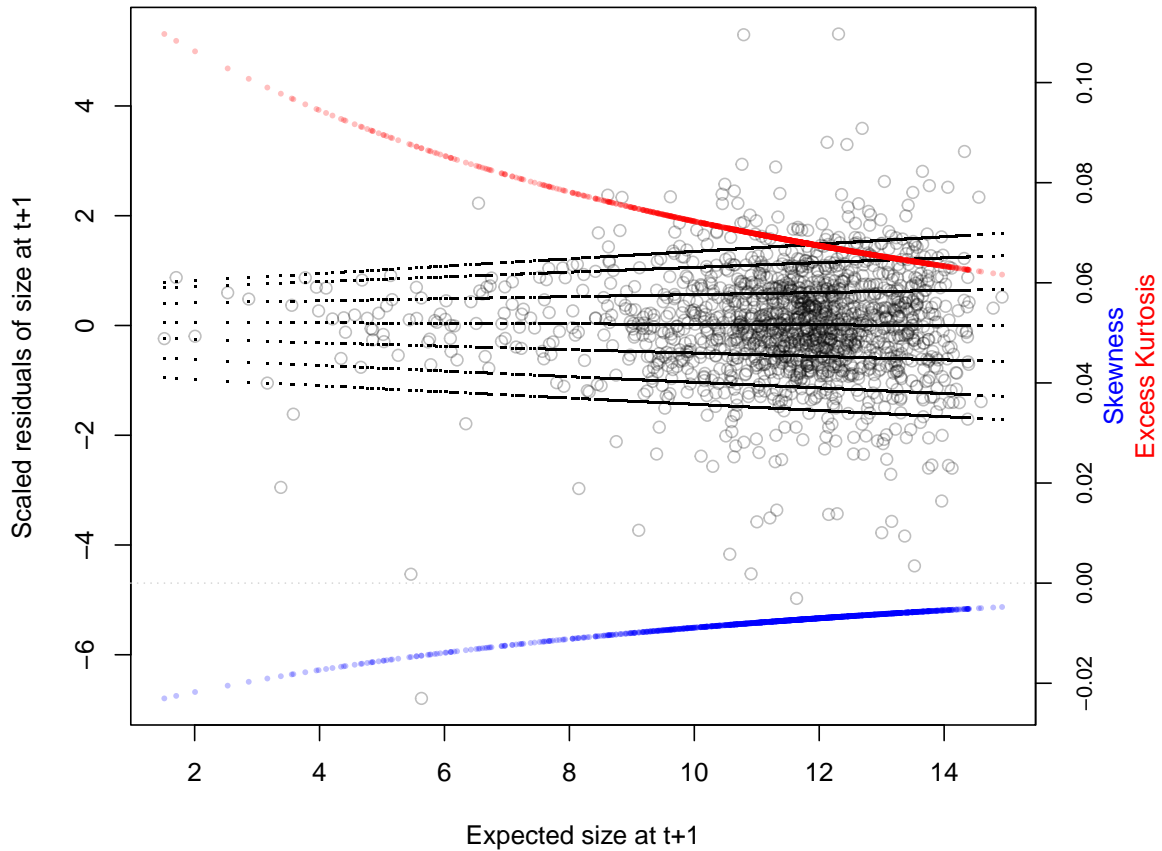


Figure 9:

493 growth modeling. We fit a custom maximum likelihood model that borrows the pieces  
 494 of the best Gaussian model that we are happy with (mean and standard deviation), lim-  
 495 iting estimation of free parameters to those that control the JSU's skewness and kurtosis.  
 496 Here is what such a hybrid likelihood model looks like in practice:

```
497 ## log_volume_t1 are the size obervations
498 ## GAU_fitted are the expected values of the best Gaussian models
499 ## pars is a vector of free parameters
500 JSULogLik=function(pars){
501   dJSU(x=log_volume_t1,
502         mu=GAU_fitted,
503         sigma=exp(GAU_sd_coef[1]+GAU_sd_coef[2]*GAU_fitted),
504         nu = pars[1]+pars[2]*GAU_fitted,
505         tau = exp(pars[3]+pars[4]*GAU_fitted), log=TRUE)
```

506 }

507 The mean of the JSU is set to that of the best Gaussian model (GAU\_fitted) and the  
508 standard deviation is a function of the mean according to the coefficients (GAU\_sd\_coef)  
509 estimated through iterative re-weighting. Based on diagnostics of the standardized resid-  
510 uals (Fig. 9), JSU parameters that control skewness and kurtosis are defined as linear  
511 functions of the mean, and it is these coefficients that are estimated by maximum likeli-  
512 hood. If it seems a little strange to swap in the fitted values from a Gaussian model as  
513 the mean of a non-Gaussian model – well, it is. Here we are relying on the robustness of  
514 linear models to deviations from normality. Alternatively, it is possible re-fit the mean  
515 and standard deviation of the JSU, alongside skewness and kurtosis, in a maximum  
516 likelihood framework. However, incorporating random effects into a custom likelihood  
517 model is non-trivial (we provide guidance on one way to do this, using the “shrinkage”  
518 approach, in Appendix XX). Therefore a key advantage of the hybrid approach is conve-  
519 nient retention of the fitted random effects and associated variance components, which  
520 get shuttled from the Gaussian model into the non-Gaussian model without any fuss.  
521 And, if this approach does not “work” (i.e., deviations from normality biased the fitted  
522 values of the Gaussian model) one would quickly find out through the simulation step of  
523 the workflow. In our case, the hybrid JSU model performed well, generating simulated  
524 data that aligned with the real data better than the best Gaussian model, particularly in  
525 **standard deviation**<sup>5</sup> and kurtosis (Fig. 10). Note that in Fig. 10 we are plotting moments  
526 of the future size distribution with respect to initial size; this distribution is also condi-  
527 tional on local density but initial size is by far the stronger predictor of future size, so  
528 we chose this this visualization.

529 **SIPM results with a better growth model.**

## 530 **4 Discussion**

531 Here are some of the issues to be discussed.

- 532 • Modeling the mean with gam vs glm
- 533 • Modeling variance and higher moments as functions of covariates vs fitted values
- 534 • Choosing a better distribution – how to make the choice
- 535 • Comparison of our method with beta regression
- 536 • We have emphasize growth but same principles apply to other continuous state  
537 transitions, eg disease IPMs.

---

<sup>5</sup>I am a little mystified as to why the JSU is so much better. It is literally the same SD in both distributions.

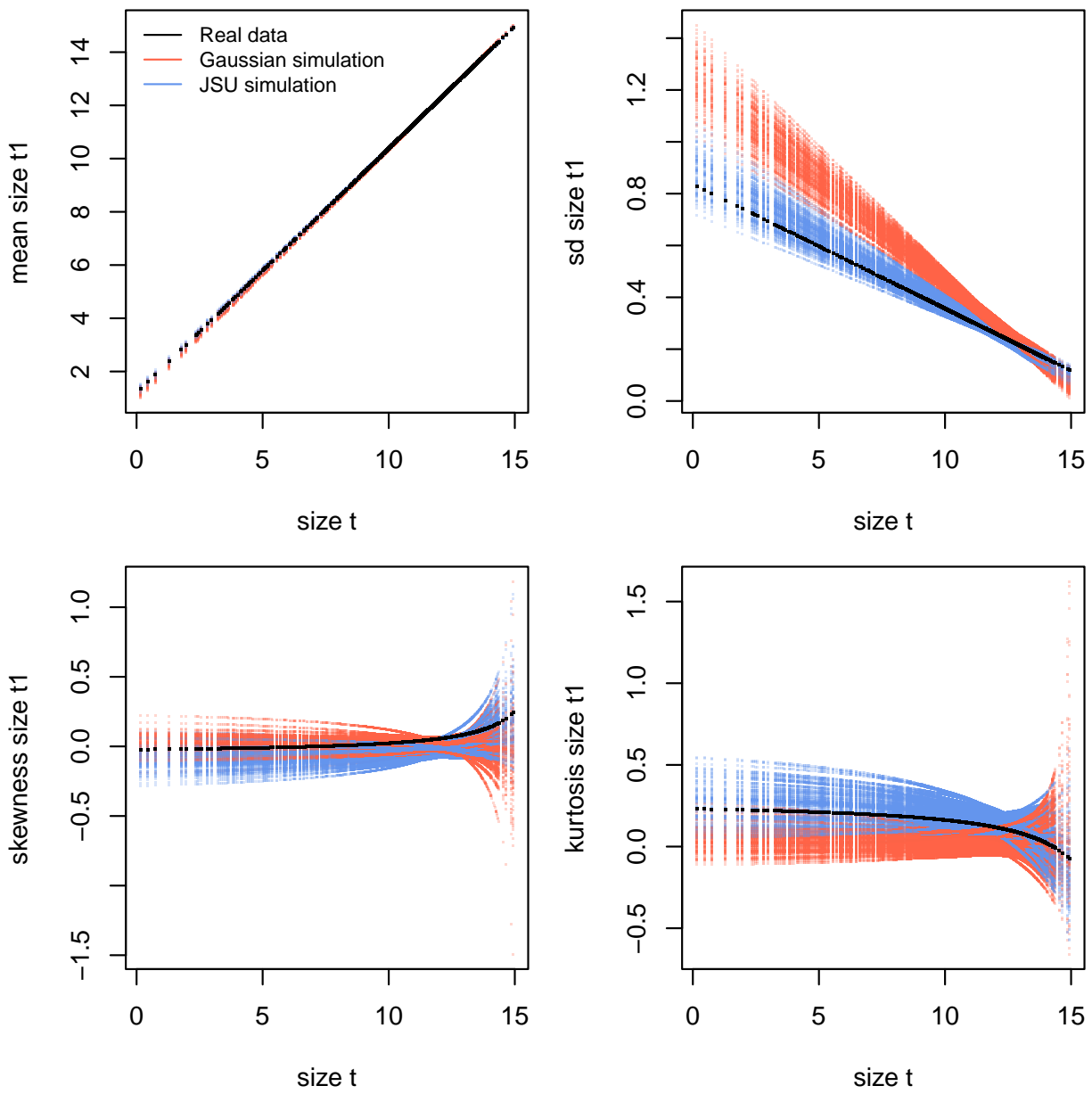


Figure 10:

## 538 Acknowledgements

539 This research was supported by US NSF grants DEB-1933497 (SPE) and ....

540 **5 Authorship statement**

541 All authors discussed all aspects of the research and contributed to developing methods,  
542 analyzing data, and writing and revising the paper.

543 **6 Data accessibility statement**

544 No original data appear in this paper. Should the paper be accepted, all computer scripts  
545 supporting the results will be archived in a Zenodo package, with the DOI included at  
546 the end of the article. During peer review, our data and code are available at [https://github.com/texmiller/IPM\\_size\\_transitions](https://github.com/texmiller/IPM_size_transitions).  
547

548 **Literature Cited**

- 549 Anscombe, F. J. and Glynn, W. J. (1983). Distribution of the kurtosis statistic  $b_2$  for  
550 normal samples. *Biometrika*, 70(1):227–234.
- 551 Bates, D., Sarkar, D., Bates, M. D., and Matrix, L. (2007). The lme4 package. *R package  
552 version*, 2(1):74.
- 553 Bruno, J. F., Ellner, S. P., Vu, I., Kim, K., and Harvell, C. D. (2011). Impacts of aspergillosis  
554 on sea fan coral demography: modeling a moving target. *Ecological Monographs*,  
555 81(1):123–139.
- 556 Compagnoni, A., Bibian, A. J., Ochocki, B. M., Rogers, H. S., Schultz, E. L., Sneck, M. E.,  
557 Elderd, B. D., Iler, A. M., Inouye, D. W., Jacquemyn, H., et al. (2016). The effect of  
558 demographic correlations on the stochastic population dynamics of perennial plants.  
559 *Ecological Monographs*, 86(4):480–494.
- 560 Conn, P. B., Johnson, D. S., Williams, P. J., Melin, S. R., and Hooten, M. B. (2018). A guide  
561 to bayesian model checking for ecologists. *Ecological Monographs*, 88(4):526–542.
- 562 Cooch, E. G. and White, G. C. (2020, accessed 5/17/2020). *Program MARK - a 'gentle  
563 introduction'*. Available at phidot.org.
- 564 Coulson, T. (2012). Integral projections models, their construction and use in posing  
565 hypotheses in ecology. *Oikos*, 121(9):1337–1350.
- 566 Crone, E. E. (2016). Contrasting effects of spatial heterogeneity and environmental  
567 stochasticity on population dynamics of a perennial wildflower. *Journal of Ecology*,  
568 104(2):281–291.
- 569 Czachura, K. and Miller, T. E. (2020). Demographic back-casting reveals that subtle  
570 dimensions of climate change have strong effects on population viability. *Journal of  
571 Ecology*.
- 572 D'Agostino, R. B. (1970). Transformation to normality of the null distribution of  $g_1$ .  
573 *Biometrika*, pages 679–681.
- 574 Davis, C. (2015). *sgt: Skewed Generalized T Distribution Tree*. R package version 2.0.
- 575 Drees, T., Ochocki, B. M., Collins, S. L., and Miller, T. E. (2023). Demography and  
576 dispersal at a grass-shrub ecotone: a spatial integral projection model for woody plant  
577 encroachment. *Ecological Monographs*, page e1574.

- 578 Easterling, M. R., Ellner, S. P., and Dixon, P. M. (2000). Size-specific sensitivity: applying  
579 a new structured population model. *Ecology*, 81(3):694–708.
- 580 Elderd, B. D. and Miller, T. E. (2016). Quantifying demographic uncertainty: Bayesian  
581 methods for integral projection models. *Ecological Monographs*, 86(1):125–144.
- 582 Ellis, M. M. and Crone, E. E. (2013). The role of transient dynamics in stochastic popula-  
583 tion growth for nine perennial plants. *Ecology*, 94(8):1681–1686.
- 584 Ellner, S. P., Adler, P. B., Childs, D. Z., Hooker, G., Miller, T. E., and Rees, M. (2022).  
585 A critical comparison of integral projection and matrix projection models for demo-  
586 graphic analysis: Comment. *Ecology*, 103(10):e3605.
- 587 Ellner, S. P., Childs, D. Z., and Rees, M. (2016). *Data-driven Modeling of Structured Popula-  
588 tions: A Practical Guide to the Integral Projection Model*. Springer, New York.
- 589 Gould, W. R. and Nichols, J. D. (1998). Estimation of temporal variability of survival in  
590 animal populations. *Ecology*, 79:2531 – 2538.
- 591 Gu, C. (2013). *Smoothing Spline ANOVA Models*. Springer Science+Business Media, New  
592 York, 2 edition.
- 593 Hadfield, J. D. et al. (2010). Mcmc methods for multi-response generalized linear mixed  
594 models: the mcmcglmm r package. *Journal of Statistical Software*, 33(2):1–22.
- 595 Héault, B., Bachelot, B., Poorter, L., Rossi, V., Bongers, F., Chave, J., Paine, C. T., Wagner,  
596 F., and Baraloto, C. (2011). Functional traits shape ontogenetic growth trajectories of  
597 rain forest tree species. *Journal of ecology*, 99(6):1431–1440.
- 598 Jones, M. and Pewsey, A. (2009). *Biometrika*, 96:761 – 780.
- 599 Jones, M. C., Rosco, J. F., and Pewsey, A. (2011). Skewness-invariant measures of kurtosis.  
600 *The American Statistician*, 65(2):89 – 95.
- 601 Komsta, L. and Novomestky, F. (2015). Moments, cumulants, skewness, kurtosis and  
602 related tests. *R package version*, 14(1).
- 603 Link, W. A. and Nichols, J. D. (1994). On the importance of sampling variance to inves-  
604 tigations of temporal variation in animal population size. *Oikos*, 69(3):539 – 544.
- 605 Louthan, A. M., Keighron, M., Kiekebusch, E., Cayton, H., Terando, A., and Morris, W. F.  
606 (2022). Climate change weakens the impact of disturbance interval on the growth rate  
607 of natural populations of venus flytrap. *Ecological Monographs*, 92(4):e1528.

- 608 McGillivray, H. (1986). Skewness and asymmetry: measures and orderings. *Annals of*  
609 *Statistics*, 14:994–1011.
- 610 Metcalf, C. J. E., Ellner, S. P., Childs, D. Z., Salguero-Gómez, R., Merow, C., McMahon,  
611 S. M., Jongejans, E., and Rees, M. (2015). Statistical modelling of annual variation for  
612 inference on stochastic population dynamics using Integral Projection Models. *Methods*  
613 *in Ecology and Evolution*, 6:1007–1017.
- 614 Miller, T. E. (2020). Long-term study of tree cholla demography in the los pinos  
615 mountains, sevilleta national wildlife refuge. [https://doi.org/10.6073/pasta/  
616 dd06df3f950afe4a4642306182237d13](https://doi.org/10.6073/pasta/dd06df3f950afe4a4642306182237d13).
- 617 Miller, T. E., Louda, S. M., Rose, K. A., and Eckberg, J. O. (2009). Impacts of insect  
618 herbivory on cactus population dynamics: experimental demography across an envi-  
619 ronmental gradient. *Ecological Monographs*, 79(1):155–172.
- 620 Ochocki, B. M., Drees, T., and Miller, T. E. (2023). Density-dependent demography of  
621 creosote bush (*larrea tridentata*) along grass-shrub ecotones. [https://doi.org/10.  
622 6073/pasta/ca53c16f16dcf9fb11f3ee99ea5445ac](https://doi.org/10.6073/pasta/ca53c16f16dcf9fb11f3ee99ea5445ac).
- 623 Ohm, J. R. and Miller, T. E. (2014). Balancing anti-herbivore benefits and anti-pollinator  
624 costs of defensive mutualists. *Ecology*, 95(10):2924–2935.
- 625 Ozgul, A., Childs, D. Z., Oli, M. K., Armitage, K. B., Blumstein, D. T., Olson, L. E., Tul-  
626 japurkar, S., and Coulson, T. (2010). Coupled dynamics of body mass and population  
627 growth in response to environmental change. *Nature*, 466(7305):482–485.
- 628 Peterson, M. L., Morris, W., Linares, C., and Doak, D. (2019). Improving structured  
629 population models with more realistic representations of non-normal growth. *Methods*  
630 *in Ecology and Evolution*, 10(9):1431–1444.
- 631 Plard, F., Schindler, S., Arlettaz, R., and Schaub, M. (2018). Sex-specific heterogene-  
632 ity in fixed morphological traits influences individual fitness in a monogamous bird  
633 population. *The American Naturalist*, 191(1):106–119.
- 634 Rees, M., Childs, D. Z., and Ellner, S. P. (2014). Building integral projection models: a  
635 user's guide. *Journal of Animal Ecology*, 83(3):528–545.
- 636 Rigby, R. A., Stasinopoulos, M. D., Heller, G. Z., and De Bastiani, F. (2019). *Distributions*  
637 *for modeling location, scale, and shape: Using GAMLSS in R*. CRC press.

- 638 Salguero-Gómez, R. and Casper, B. B. (2010). Keeping plant shrinkage in the demo-  
639 graphic loop. *Journal of Ecology*, 98(2):312–323.
- 640 Schielzeth, H., Dingemanse, N. J., Nakagawa, S., Westneat, D. F., Allegue, H., Teplitsky,  
641 C., Réale, D., Dochtermann, N. A., Garamszegi, L. Z., and Araya-Ajoy, Y. G. (2020).  
642 Robustness of linear mixed-effects models to violations of distributional assumptions.  
643 *Methods in ecology and evolution*, 11(9):1141–1152.
- 644 Schultz, E. L., Eckberg, J. O., Berg, S. S., Louda, S. M., and Miller, T. E. (2017). Native  
645 insect herbivory overwhelms context dependence to limit complex invasion dynamics  
646 of exotic weeds. *Ecology letters*, 20(11):1374–1384.
- 647 Stasinopoulos, D. M., Rigby, R. A., et al. (2007). Generalized additive models for location  
648 scale and shape (gamlss) in r. *Journal of Statistical Software*, 23(7):1–46.
- 649 Stubberud, M. W., Vindenes, Y., Vøllestad, L. A., Winfield, I. J., Stenseth, N. C., and Lan-  
650 gangen, Ø. (2019). Effects of size-and sex-selective harvesting: An integral projection  
651 model approach. *Ecology and Evolution*, 9(22):12556–12570.
- 652 Wan, X., Wang, W., Liu, J., and Tong, T. (2014). Estimating the sample mean and stan-  
653 dard deviation from the sample size, median, range and/or interquartile range. *BMC  
654 medical research methodology*, 14:1–13.
- 655 Williams, J. L., Miller, T. E., and Ellner, S. P. (2012). Avoiding unintentional eviction from  
656 integral projection models. *Ecology*, 93(9):2008–2014.
- 657 Wood, S. (2017). *Generalized Additive Models: An Introduction with R*. Chapman and  
658 Hall/CRC, 2 edition.
- 659 Zhang, J. L. (2014). Comparative investigation of three bayesian p values. *Computational  
660 Statistics & Data Analysis*, 79:277–291.

# Appendices

## S.1 The Jones-Pewsey distribution

Jones and Pewsey (2009) introduced a simple, tractable generalization of the Normal distribution with two additional parameters determining asymmetry (skewness), and tail weight (kurtosis) which can be either lighter or heavier than the Gaussian. It is defined as a transformation of a  $\text{Normal}(0,1)$  random variable using the hyperbolic sine function ( $\sinh$ ) and its inverse ( $\text{asinh}$ ), as follows. The distribution family's base probability density  $f_{\epsilon,\delta}$  is the probability density of the random variable  $X_{\epsilon,\delta}$  where

$$Z = \sinh(\delta \text{ asinh}(X_{\epsilon,\delta}) - \epsilon) \quad (\text{S.1})$$

and  $Z$  has a  $\text{Normal}(0,1)$  distribution. Equivalently,

$$X_{\epsilon,\delta} = \sinh\left(\frac{1}{\delta} \text{ asinh}(Z) + \frac{\epsilon}{\delta}\right). \quad (\text{S.2})$$

Parameters  $\delta = 1, \epsilon = 0$  give the  $\text{Normal}(0,1)$  distribution. Skewness has the sign of  $\epsilon$ , and  $\delta > 0$  controls tail weight, with heavier than Gaussian tails for  $\delta < 1$  and lighter than Gaussian tails for  $\delta > 1$ . A formula for the density  $f_{\epsilon,\delta}$  is given by Jones and Pewsey (2009, eqn. 2). The general four-parameter family with location parameter  $\mu$  and scale parameter  $\sigma$  is defined as the probability densities of  $\mu + \sigma X_{\epsilon,\delta}$ . We refer to this as the JP distribution family.

As is unfortunately the case for most four-parameter distributions  $\mu$  is not the mean,  $\sigma$  is not the standard deviation,  $\epsilon$  is not the skew and  $\delta$  is not the kurtosis. All else being equal, larger  $\mu$  gives a larger mean, larger  $\sigma$  gives a higher standard deviation, higher  $\epsilon$  gives higher asymmetry, and higher  $\delta$  gives heavier tail weight. But each moment is jointly determined by all four parameters.

The main advantage of the JP distribution is that the attainable combinations of skewness and kurtosis are very broad, compared to other four-parameter families, and come very close to the theoretical limits on kurtosis as a function of skewness (Jones and Pewsey, 2009, Fig. 2). Additionally, being a transformation of the Normal makes it very simple to generate random numbers from the distribution, and to compute probability density, cumulative distribution, and quantile functions. There are also simple analytic formulas for the first four moments (Jones and Pewsey, 2009, p. 764) which we use below

689 to define a centered and scaled version in which  $\mu$  and  $\sigma$  are the mean and standard  
690 deviation.

691 The definition (S.2) shows that the distribution depends on  $\epsilon$  only through the ratio  
692  $\epsilon/\delta$ . We have found that this property can be problematic for estimating distribution  
693 parameters. Even with good sized ( $n = 250$  or  $500$ ) data sets generated from the distri-  
694 bution with known parameters, both maximum likelihood and Bayesian estimation were  
695 unstable for some values of  $\epsilon$  and  $\delta$ , occasionally yielding estimates far from the truth.  
696 One cause was a ridge in the  $(\epsilon, \delta)$  likelihood surface with a constant of  $\epsilon/\delta$ . Another is  
697 that when  $\delta$  is large, changes in  $\epsilon$  have little effect.

698 To avoid that problems, we reparameterize the distribution as follows:

699 
$$X_{\lambda, \tau} = \sinh(e^{-\tau} \operatorname{asinh}(Z) + \lambda). \quad (\text{S.3})$$

700 Thus, the two parameterizations are related by

701 
$$\delta = e^\tau, \epsilon = \delta\lambda = e^\tau\lambda. \quad (\text{S.4})$$

702 The definition of  $\tau$  allows it to take any real value, with negative values giving thinner  
703 than Gaussian tails and positive values giving fatter than Gaussian tails.  $\lambda$  also can take  
704 any real value, and the distribution's skew has the same sign as  $\lambda$ . Because the  $\sinh$   
705 function is nonlinear, it is still the case that the skew depends on  $\tau$  as well as  $\lambda$ , but the  
706 "crosstalk" between the kurtosis and skew parameters is weaker. As a result, we found  
707 that maximum likelihood estimation of parameter values was generally more reliable if  
708 the distribution is parameterized in terms of  $\tau$  and  $\lambda$ .

## 709 S.2 Estimating mixed-effects models using shrinkage

710 Ecologists often fit demographic and other statistical models that include random effects  
711 terms to quantify variation among years, spatial locations, individuals, etc. Random  
712 effects are a natural choice when interest centers on the magnitude of variation (e.g., how  
713 much does mortality vary among years?) rather than individual values (e.g., mortality  
714 in 2013). They also allow each estimate to "borrows strength" from others, so that (for  
715 example) the estimate from a year with small sample size (and thus large sampling  
716 variability) is shifted towards the center of the overall distribution.

717 Specialized software is often used to fit such models, such as the **nlme**, **lme4**, **mgee**  
718 and **gamm4** libraries in R, but these only allow a small subset of the distribution families

we want to consider for modeling growth increments (the **gamlss** package allows many distribution families, but in our experience, even when random effects are simple in structure the fitting algorithms often fail to converge or fail to find the global optimum).

One way past this limitation is Bayesian estimation, using STAN with user-written (or borrowed) code for the chosen growth distribution (see section XX for an example). In this appendix we describe another option, introduced by Link and Nichols (1994) and Gould and Nichols (1998): fitting a fixed-effects model by Maximum Likelihood, followed by shrinkage of coefficient estimates. None of the ideas here are original. The material overlaps Appendix S1 of Metcalf et al. (2015), but for completeness we make it self-contained. Appendix D of Cooch and White (2020) (written by K.D. Burnham) provides more details and examples in the context of capture-recapture analysis.

Here we explain shrinkage using a simple model based on our analysis of *Pseudoeugenia spicata*. That model includes random effects for between-year variation in the slope and intercept of future size (log area) as a function of initial size. To keep the example simple, we assume that initial size and year are the only covariates, and we assume that growth increments follow a skew-Normal distribution with nonconstant variance and constant skew parameter. Code for this example is in the script `SimpleShrinkageExample.R`. The first part of the script generates an artificial data set by fitting the model to a subset of the growth data (20th century Control plots), and randomly generating new “size next year” values for each individual in the actual data set. The second part contains the “data” analysis.

As in our *P. spicata* analysis, we assumed that that the skew and kurtosis parameters were functions of the location parameter; this dominated ( $\Delta AIC \approx 30$ ) the alternate model with skew and kurtosis depending on initial size. The analogous Gaussian model, with constant variance, could be fitted as follows using `lmer`:

```
744 lmer(new.size ~ init.size + (init.size|year), data=growthData, REML=TRUE);  
745 where growthData is a data frame holding the data with year as an unordered factor.  
746 For our skew-Normal model, we instead use maximum likelihood with all between-year  
747 variation included as fixed effects. The appropriate design matrix is easily constructed  
748 using the model.matrix function:
```

```
749 U = model.matrix(~ year + init.size:year - 1, data=growthData)
```

If there are  $T$  years, the matrix  $U$  specified in this way has  $2T$  columns corresponding to  $n$  annual intercepts and  $T$  annual slopes.

752 Using this design matrix, we can readily write a log likelihood function for use with  
 753 the **maxLik** package, with a log link function for the variance because it is necessarily  
 754 positive:

```
755 LogLik=function(pars,new.size,U){  

    756     pars1 = pars[1:ncol(U)]; pars2=pars[-(1:ncol(U))];  

    757     mu = U%*%pars1;  

    758     sigma = exp(pars2[1]+pars2[2]*mu);  

    759     dSN1(new.size, mu=mu, sigma=sigma, nu=pars2[3], log=TRUE)  

    760 }
```

761 Parameters and their standard errors can then be estimated with **maxLik**, starting  
 762 from a random guess:

```
763 start=c(runif(ncol(U)), rep(0,3))  

    764 out=maxLik(logLik=LogLik,start=start, new.size=simData$new.size,U=U,  

    765     method="BHHH",control=list(iterlim=5000,printLevel=1),finalHessian=TRUE);  

    766 coefs = out$estimate; # parameters  

    767 V = vcov(out); SEs = sqrt(diag(V)); # standard errors
```

768 In real life we would repeat the optimization several times with several different starting  
 769 values, to be confident that the optimal parameter values had been found.

770 Focus now on the year-specific intercept parameters  $\hat{a}_t, t = 1, 2, \dots, T$ . We can view  
 771 the year-specific estimates  $\hat{a}_t$  as consisting of unobserved true values  $a_t$  plus sampling  
 772 error:

$$\hat{a}_t = a_t + \varepsilon_t \quad (\text{S.5})$$

774 Because of the sampling errors, the sample variance of the estimates  $\hat{a}_t$  is an upward-  
 775 biased estimate of the true across-year variance in the parameter. That is undesirable if  
 776 the model will be used to project how temporal variability affects population dynamics.  
 777 However, maximum likelihood estimation gives us an approximate variance-covariance  
 778 matrix  $\hat{V}$  of the sampling errors,  $V$  in the code above. With that information, we can  
 779 estimate the parameters of a random effects model for the intercept parameters, and  
 780 thereby improve the year-specific estimates and the estimate of the across-year variance.

781 The model is as follows. We make the standard mixed-models assumptions that the  
 782  $a_t$  are drawn independently from some fixed distribution with unknown variance  $\sigma^2$ .  
 783 We also assume that the estimates  $\hat{a}_t$  are unbiased, that is

$$784 \mathbb{E}(\varepsilon_t | a_t) = 0. \quad (\text{S.6})$$

785 These are optimistic assumptions, but not excessively optimistic. Some degree of tem-  
 786 poral correlation will often be present, and as we explain at the end, it is theoretically  
 787 possible to account for it. Maximum likelihood parameter estimates are not unbiased,  
 788 but if the assumptions of maximum likelihood are satisfied the bias is asymptotically  
 789 negligible compared to the standard error (the bias scales as the inverse of sample size,  
 790 the standard error as the square root of the inverse of sample size).

791 Let  $S^2$  denote the sample variance of the estimates  $\hat{a}_t$ . It can then be shown that

$$792 \quad \mathbb{E}(S^2) = \sigma^2 + \frac{1}{T} \sum_{t=1}^T \mathbb{E}Var(\varepsilon_t) - \frac{1}{T(T-1)} \sum_{i=1}^{j-1} \sum_{j=1}^T \mathbb{E}Cov(\varepsilon_i, \varepsilon_j). \quad (\text{S.7})$$

793 This is eqn. (1) in Gould and Nichols (1998) in our notation, without the term that results  
 794 from temporal autocorrelation.

795 The terms besides  $\sigma^2$  on the right-hand are the expected impact of sampling error  
 796 on the across-year variance of the parameter estimates; their presence makes  $S^2$  a biased  
 797 estimate of  $\sigma^2$ . However, all of those terms correspond to entries in the variance-  
 798 covariance matrix  $V$ . We can therefore use our estimated variance-covariance matrix  $\hat{V}$   
 799 to remove the bias due to sampling variability:

$$800 \quad \hat{\sigma}^2 = S^2 - \frac{1}{T} \sum_{t=1}^T \hat{V}_{t,t} + \frac{1}{T(T-1)} \sum_{i=1}^{j-1} \sum_{j=1}^T \hat{V}_{i,j}. \quad (\text{S.8})$$

801  $\hat{\sigma}^2$  estimates the variance of the distribution from which the  $a_t$  are assumed to be drawn.

802 Using that estimate, we can adjust the year-specific estimates to reduce the ex-  
 803 pected impact of sampling error. Depending on your purposes, there are two possible  
 804 adjustments. The first option is the one used in the popular capture-recapture analysis  
 805 software Mark Cooch and White (2020),

$$806 \quad \tilde{a}_t = \bar{a}_t + \sqrt{\frac{\hat{\sigma}^2}{\hat{\sigma}^2 + \hat{V}_{t,t}}} (\hat{a}_t - \bar{a}_t). \quad (\text{S.9})$$

807 The name “shrinkage” comes from the fact that each estimate is adjusted towards the  
 808 overall mean, with larger adjustments of values that have higher estimated sampling  
 809 error variance,  $\hat{V}_{t,t}$ . This shrinkage estimate has the property that the expected sample  
 810 variance of the adjusted estimates  $\tilde{a}_t$  is very close to  $\hat{\sigma}^2$ , so the  $\tilde{a}_t$  approximate the actual  
 811 amount of parameter variation.

812        The second is to replace  $\hat{a}_t$  by the least-squares estimate of  $a_t$  under the additional  
 813        assumption that the  $a_t$  are drawn from a Gaussian distribution; this is given by

$$814 \quad \tilde{a}_t = \bar{a}_t + \frac{\hat{\sigma}^2}{\hat{\sigma}^2 + \hat{V}_{t,t}} (\hat{a}_t - \bar{a}_t). \quad (\text{S.10})$$

815        This option is theoretically preferable if the Gaussian assumption is reasonable, and you  
 816        are more interested in year-specific values rather than across-year variance. However,  
 817        Metcalf et al. (2015) found that even (S.9), which does less shrinkage, resulted in a small  
 818        downward bias in the temporal variance of population growth rates. This argues for  
 819        always using the first option, and we do the same here.

820        We differ from MARK, however, in using (S.8) rather than an iterative method  
 821        that takes (S.8) as its starting estimate and refines the estimate by using weighted least  
 822        squares based on the current estimate. Metcalf et al. (2015) found, in simulation studies,  
 823        that the iterative method was either slightly beneficial or wildly inaccurate. We therefore  
 824        advise against it.

825        Finally, as mentioned above, the estimate of  $\sigma^2$  can account for temporal autocor-  
 826        relation in the  $a_t$ . When present, those correlations add a term to eqn. (S.7) (see eqn.  
 827        (1) in Gould and Nichols (1998)), which can be estimated from the sample autocorre-  
 828        lation of the  $\hat{a}_t$ . We do not recommend doing this (and therefore omit the formulas)  
 829        because the autocorrelations can only be reliably estimated if they fall to nearly zero  
 830        within lag  $m \ll T$ , in which case the autocorrelation term is small (specifically,  $O(m/T)$ ).  
 831        Otherwise, the random error from using poorly estimated autocorrelations is likely to  
 832        outweigh the small bias from omitting that term.

833        The take-home message is that estimating random effects from the regression coef-  
 834        ficients is very simple:

```
835 # Variance-covariance matrices for intercepts and slopes
836 V1 = V[1:T,1:T]; V2 = V[(T+1):(2*T),(T+1):(2*T)];
837 # Extract year-specific intercepts, center them to zero
838 fixed.fx = coefs[1:T]; fixed.fx = fixed.fx-mean(fixed.fx);
839
840 # Estimate sigma^2
841 var.hat = mean(fixed.fx^2) - mean(diag(V1)) +
842           (sum(V1)-sum(diag(V1)))/(2*T*(T-1));
843
844 # Shrink deviations from the mean
```

```

845 shrinkRanIntercept = fixed.fx*sqrt(var.hat/(var.hat + diag(V1)));
846
847 # Do it all again for the slopes
848 fixed.fx2 = coefs[(T+1):(2*T)]; fixed.fx2 = fixed.fx2-mean(fixed.fx2);
849 var2.hat = mean(fixed.fx2^2) - mean(diag(V2)) +
850   (sum(V2)-sum(diag(V2)))/(2*T*(T-1));
851 shrinkRanSlope = fixed.fx2*sqrt(var2.hat/(var2.hat + diag(V2)));

```

852 The figure below shows the results for one artificial PSSP “data” set, having  $T = 22$   
853 years and growth measurements on about 175 individuals/year on average. The true  
854 random year effects (the ones used to generate the data) are recovered with good accu-  
855 racy and no bias. In particular there is no sign of extreme values being pulled in too  
856 far towards the mean, which would cause an S-shaped graph of estimated versus true  
857 values.

